Biofilm 7 (2024) 100185

Contents lists available at ScienceDirect

Biofilm

journal homepage: www.sciencedirect.com/journal/biofilm

The use of biomimetic surfaces to reduce single- and dual-species biofilms of *Escherichia coli* and *Pseudomonas putida*

Rita Teixeira-Santos [a,b], Ana Azevedo [a,b], Maria J. Romeu [a,b], Cristina I. Amador [c], Luciana C. Gomes [a,b], Kathryn A. Whitehead [d], Jelmer Sjollema [e], Mette Burmølle [c], Filipe J. Mergulhão [a,b,*]

[a] *LEPABE – Laboratory for Process Engineering, Environment, Biotechnology and Energy, Faculty of Engineering, University of Porto, Rua Dr. Roberto Frias, 4200-465, Porto, Portugal*
[b] *ALiCE – Associate Laboratory in Chemical Engineering, Faculty of Engineering, University of Porto, Rua Dr. Roberto Frias, 4200-465, Porto, Portugal*
[c] *Section of Microbiology, Department of Biology, University of Copenhagen, Universitetsparken 15, 2100, Copenhagen, Denmark*
[d] *Microbiology at Interfaces, Manchester Metropolitan University, Manchester, M15GD, UK*
[e] *Department of Biomedical Engineering, University of Groningen, University Medical Center Groningen, Groningen, the Netherlands*

ARTICLE INFO

Keywords:
Biomimetic surfaces
Topographical features
Hydrophobicity
Antiadhesive effect
Antibiofilm activity
Food contact surfaces

ABSTRACT

The ability of bacteria to adhere to and form biofilms on food contact surfaces poses serious challenges, as these may lead to the cross-contamination of food products. Biomimetic topographic surface modifications have been explored to enhance the antifouling performance of materials. In this study, the topography of two plant leaves, *Brassica oleracea* var. *botrytis* (cauliflower, CF) and *Brassica oleracea capitate* (white cabbage, WC), was replicated through wax moulding, and their antibiofilm potential was tested against single- and dual-species biofilms of *Escherichia coli* and *Pseudomonas putida*. Biomimetic surfaces exhibited higher roughness values ($S_{a\ WC} = 4.0 \pm 1.0$ μm and $S_{a\ CF} = 3.3 \pm 1.0$ μm) than the flat control ($S_{a\ F} = 0.6 \pm 0.2$ μm), whilst the CF surface demonstrated a lower interfacial free energy (ΔG_{iwi}) than the WC surface (-100.08 mJ m^{-2} and -71.98 mJ m^{-2}, respectively). The CF and WC surfaces had similar antibiofilm effects against single-species biofilms, achieving cell reductions of approximately 50% and 60% for *E. coli* and *P. putida*, respectively, compared to the control. Additionally, the biomimetic surfaces led to reductions of up to 60% in biovolume, 45% in thickness, and 60% in the surface coverage of single-species biofilms. For dual-species biofilms, only the *E. coli* strain growing on the WC surface exhibited a significant decrease in the cell count. However, confocal microscopy analysis revealed a 60% reduction in the total biovolume and surface coverage of mixed biofilms developed on both biomimetic surfaces. Furthermore, dual-species biofilms were mainly composed of *P. putida*, which reduced *E. coli* growth. Altogether, these results demonstrate that the surface properties of CF and WC biomimetic surfaces have the potential for reducing biofilm formation.

1. Introduction

The adhesion of bacteria and subsequent biofilm formation on food contact surfaces poses major concerns, as biofilms act as reservoirs for pathogenic and spoilage microorganisms that potentially contaminate raw materials and food products during processing [1–3]. This may lead to substantial economic losses for the industry arising from food spoilage and an increased risk of foodborne illnesses for consumers [3]. Among the parameters affecting biofilm formation, equipment design and material surface properties (e.g., topography and physicochemistry) play major roles in bacterial binding, which is the pre-requisite to biofilm formation. In the food industry, persistent bacteria may colonise surfaces under static conditions, such as on equipment that is intermittently used, for example, the inside of mixing tanks, vats, and tubing, and this

* Corresponding author. LEPABE – Laboratory for Process Engineering, Environment, Biotechnology and Energy, Faculty of Engineering, University of Porto, Rua Dr. Roberto Frias, 4200-465, Porto, Portugal.
E-mail addresses: ritadtsantos@fe.up.pt (R. Teixeira-Santos), acma@fe.up.pt (A. Azevedo), mariaromeu@fe.up.pt (M.J. Romeu), chierro@bio.ku.dk (C.I. Amador), luciana.gomes@fe.up.pt (L.C. Gomes), k.a.whitehead@mmu.ac.uk (K.A. Whitehead), j.sjollema@umcg.nl (J. Sjollema), burmolle@bio.ku.dk (M. Burmølle), filipem@fe.up.pt (F.J. Mergulhão).

https://doi.org/10.1016/j.bioflm.2024.100185
Received 14 December 2023; Received in revised form 26 January 2024; Accepted 16 February 2024
Available online 21 February 2024

may occur at ambient temperature or in refrigerated conditions. Poor design features encountered in such tanks make surface contamination, including biofilms, difficult to remove [4].

Biofilms are complex communities of microbial cells surrounded by a self-produced matrix of extracellular polymeric substances [5–8]. This matrix confers additional protection to microorganisms against adverse conditions, such as exposure to disinfectants or antimicrobial agents [9]. Consequently, these well-structured communities enhance the ability of pathogenic and spoilage bacteria to persist in food environments, compromising food safety and quality despite the implementation of decontamination procedures and strict hygiene measures [2,10].

Due to the species diversity present in raw materials, biofilms found on food contact surfaces are often formed by two or more species of bacteria [3,11,12]. Foodborne bacteria include *Staphylococcus* spp., *Streptococcus* spp., *Pseudomonas* spp., *Acinetobacter* spp., *Escherichia coli*, *Listeria monocytogenes*, and *Salmonella enteritidis* [12,13]. Multi-species biofilm formation is affected by surface properties, food matrix components, environmental conditions, and the bacteria involved [14]. In these biofilms, bacteria coexist in proximity to other species and their interactions may have synergistic, indifferent or antagonistic impacts on resident microorganisms [2,12,15]. Therefore, interspecies interactions influence both the structure and functionality of microbial communities [16]. Generally, synergistic interactions can enhance the formation of biofilms and increase cell numbers, indifferent interactions cause no change in biofilm production or cell numbers whilst antagonistic interactions may inhibit the growth of one or more species [3,17–20]. Nevertheless, multi-species biofilms are mostly described as being more resistant to biofilm control strategies than single-species biofilms (e.g., disinfection processes) [21,22].

Despite the implementation of cleaning and disinfection procedures and the selection of surface materials, biofilm control in the food industry remains a significant challenge [3,23,24]. Therefore, it is crucial to develop strategies to delay biofilm formation, thus potentially increasing operational time, reducing the use of cleaning materials, and ultimately saving water and electricity.

Surface modification is a promising approach that has been explored to prevent bacterial adhesion and mitigate biofilm formation in various industries, including food processing and healthcare. Several strategies have been applied to change the chemistry and morphology of material surfaces, including mimicking natural micro- and nanostructures on artificial surfaces [25,26].

Biomimetic surfaces have gained significant attention for their exceptional properties, including self-cleaning, water-repellence, antimicrobial, and antifouling characteristics [25,27,28]. Based on the understanding that bacterial adhesion is influenced by surface energy, roughness, and wettability [29,30], biomimetic surfaces intend to replicate these attributes, reproducing topographies from nature to change bacteria-surface interactions and reduce fouling [26]. The application of biomimetic surfaces to control bacterial adhesion on food contact surfaces has already been reported [28,31]. McClements et al. [28] demonstrated that replica gladioli leaf surfaces were effective in reducing *E. coli* and *L. monocytogenes* attachment, adhesion, and retention. Additionally, in a previous study, Gomes et al. [31] revealed that the cauliflower and white cabbage biomimetic surfaces were promising in decreasing the adhesion and retention of *E. coli* and *L. monocytogenes* cells.

The present study aimed to synthesize biomimetic surfaces of *Brassica oleracea* var. *botrytis* (cauliflower, CF) and *Brassica oleracea capitate* (white cabbage, WC) leaves by wax moulding, and characterize their topographic and physicochemical properties. These plant leaves were selected based on their ability to repel water droplets [31] and because they are available all year around. Additionally, the antibiofilm performance of the synthesized surfaces was evaluated against single- and dual-species biofilms of *E. coli* and *Pseudomonas putida*. To the best of our knowledge, this is the first study exploring the antibiofilm performance of tailor-made biomimetic surfaces to control multi-species biofilms.

2. Materials and methods

2.1. Synthesis of biomimetic surfaces

Biomimetic surfaces were synthesized using CF and WC leaves as models since they present self-cleaning properties [31]. Fresh CF and WC vegetables, daily delivered in the market, were purchased and used within a 4-h time period on the same day. The surfaces were produced using a two-step casting technique, as previously described by McClements et al. [28]. In the first step, negative silicone moulds of each leaf type were produced by fixing several biological samples to a planar surface using double-sided tape and covering the adaxial leaf surfaces with duplicating silicone (Shera Duo-Sil H, Shera GmbH & Co. KGm, Lemförde, Germany). After curing, the plant leaves were carefully removed. In the second step, dental wax (Kemdent Eco dental wax, Wiltshire, UK) was poured into the negative moulds, resulting in the creation of positive wax surfaces for each leaf. Wax was chosen to synthesize the biomimetic surfaces due to its analogous physicochemical properties to several hydrophobic leaves and ease of moulding [28,32]. Flat wax surfaces (used as a control) were produced in a similar manner using a non-treated polystyrene Petri dish with low roughness (average S_a value of 8 nm [33]).

Individual circular coupons of each wax surface were obtained using a sterilized 10 mm diameter steel hole punch (coupon area ~ 79 mm^2).

2.2. Bacterial strains construction and growth conditions

A model strain of *E. coli* (CECT 434) and an industrial isolate of *P. putida* (isolated from fresh-cut salad process [34]) were used for the construction of chromosomally tagged strains expressing green fluorescent protein (GFP) and mCherry fluorochromes, respectively. Bacteria were stored at −80 °C in Lysogeny broth medium (LB; VWR, Søborg, Denmark) with 30% (v/v) glycerol. Before the experiments, strains were spread on LB agar and incubated overnight (16–18 h) at 30 °C.

2.2.1. Preparation of electrocompetent cells

Electrocompetent *E. coli* and *P. putida* cells were prepared to construct chromosomally tagged bacteria. Briefly, single colonies of each strain were inoculated in LB broth medium and incubated overnight at 30 °C with agitation. For *E. coli*, a fresh culture was prepared and incubated at 30 °C with agitation until it reached the mid-exponential phase ($OD_{600\ nm} = 0.6$). Cells were harvested by centrifugation (Eppendorf 5415D) at 3300 × *g* for 5 min at room temperature (RT). Subsequently, *E. coli* cells underwent four consecutive cycles of washing with a chilled 10% (v/v) glycerol solution and centrifugation at 3300 × *g* for 3.5 min at 4 °C [35]. For *P. putida*, the overnight culture was centrifuged at 16,000 × *g* for 2 min at RT. The cell pellet was then subjected to two cycles of washing with 300 mM sucrose (Sigma-Aldrich, Søborg, Denmark) at RT and centrifugation at 16,000 × *g* for 2 min at RT [36].

2.2.2. Transformation of E. coli and P. putida strains

The pGRG36-Plpp::gfp-Kan^R plasmid was used to integrate a cassette containing the gene encoding GFP into the chromosome of *E. coli* through Tn7 transposition, following the procedure described by McKenzie and Craig [37]. This plasmid, which is a derivative of pGRG36, contains a transcriptional fusion protein with *gfp* and transposase genes controlled by the *araBAD* promoter. Additionally, this plasmid has a temperature-sensitive origin of replication and, consequently, all incubation steps before the transposition were conducted at 30 °C. 100–150 ng of the pGRG36-Plpp::gfp-Kan^R plasmid was mixed with 50 μL of electrocompetent *E. coli* cells and subjected to electroporation in 1-mm electroporation cuvettes (MicroPulser Electroporator, Bio-Rad, Copenhagen, Denmark; 1.8 kV/cm for ~ 5 ms). As the pGRG36 derivative plasmid contains an ampicillin (Amp) resistance gene, plasmid-electroporated cells were incubated overnight on LB agar plates

supplemented with 100 μg mL^{-1} Amp (Sigma-Aldrich, Søborg, Denmark) to select the transformants. Subsequently, the transformant cells were inoculated into 5 mL of LB broth medium supplemented with 25 μg mL^{-1} kanamycin (Kan; Sigma-Aldrich, Søborg, Denmark) and 10 mM L(+)-arabinose (Sigma-Aldrich, Søborg, Denmark), and incubated at 30 °C overnight to induce the expression of the transposase. This bacterial culture was then plated on LB agar plates containing 25 μg mL^{-1} Kan and incubated overnight at 42 °C to block the replication of the pGRG36-Plpp::gfp-Kan^R plasmid. To identify the Tn7 insertion and loss of the plasmid, clones were plated on both LB agar supplemented with 25 μg mL^{-1} Kan and LB agar supplemented with 100 μg mL^{-1} Amp and incubated overnight at 37 °C. Colonies that grew on LB supplemented with Kan but not on LB supplemented with Amp corresponded to bacteria that were chromosomally tagged with GFP and did not contain the plasmid.

In turn, the Plpp::mCherry fusion was integrated into the *P. putida* chromosome using the pUC18-miniTn7-lacIq-Plpp::mcherry-Kan^R-Amp^R delivery plasmid and the pTNS2 helper plasmid harbouring the transposase genes. None of these plasmids are replicative in *Pseudomonas* spp. For that, 200 ng of both plasmids were mixed with 100 μL of electrocompetent *P. putida* cells by electroporation (1.25 kV/cm for ~ 5 ms). Plasmid-electroporated cells were incubated in fresh LB medium at 30 °C for 3 h. Subsequently, bacteria were spread on LB agar plates supplemented with 25 μg mL^{-1} Kan at 37 °C to select the transformants.

The integration of the *gfp* and *mCherry* genes into the chromosomes of *E. coli* and *P. putida*, respectively, was confirmed through flow cytometry and fluorescence microscopy. Chromosomally tagged *E. coli* CECT 434-Plpp::gfp-Kan^R and *P. putida*-lacI-Plpp::mCherry-Kan^R were successfully obtained and used in biofilm formation assays.

2.3. Surface characterization

2.3.1. Scanning electron microscopy (SEM)

The morphology of the synthesized surfaces and bacteria under study was analysed through SEM. To study bacteria, cells were cultured for 24 h, and 10 μL of each suspension were placed onto 1 cm × 1 cm silicon wafer coupons (Montco Technologies, Spring City, PA, USA). Coupons were dried in a laminar airflow cabinet for 1 h and then immersed in 4% glutaraldehyde (Agar Scientific, Stansted, UK) overnight at 4 °C. Subsequently, they were sequentially immersed in different ethanol solutions (30%, 50%, 70%, 90%, and 100%) for 10 min each and dried for 1 h. Samples were fixed to SEM tubes using conductive double-sided pads (Agar Scientific, Stansted, UK) and sputter-coated with gold in a SEM coating system (Polaron, Watford, UK). Biomimetic surfaces and bacteria were analysed using a Zeiss Supra 40VP field-emission gun scanning electron microscope (Carl Zeiss Ltd., Cambridge, UK). SEM images were obtained using SmartSEM software version 5.6 (Carl Zeiss Ltd., Cambridge, UK). At least three images from three replicates of each sample were randomly acquired at different magnifications ($n = 9$).

2.3.2. Optical profilometry

The topography of the synthesized biomimetic surfaces was assessed by optical profilometry, as previously described by Skovager et al. [38]. Surface analysis was conducted using a MicroXAM surface mapping microscope from ADE Corporation (XYZ model 4400 mL system, Tucson, AZ, USA) with a 50 × objective (170 μm × 170 μm coupon area, corresponding to a total of 0.1% of the coupon area) and coupled to an AD phase shift controller (Omniscan, Wrexham, UK). Each analysis was performed using extended-range vertical scanning interferometry. The values of average roughness (S_a), maximum peak height (S_p), maximum pit depth (S_v), and mean width of the profile elements (R_{sm}) resulted from triplicate measurements of three samples ($n = 9$) and were extracted using MountainsMap® Topography version 10.0.10433 (Digital Surf, Besançon, France). Two-dimensional (2D) topography maps were also obtained using MountainsMap® software.

2.3.3. Thermodynamic analysis

The synthesized surfaces and chromosomally tagged bacteria were thermodynamically characterized through contact angle measurements and the application of the Van Oss approach [39]. Bacterial substrata were prepared by filtering *E. coli* and *P. putida* cell suspensions (1×10^9 cells mL^{-1}) using cellulose membranes, according to the protocol developed by Busscher et al. [40]. Contact angle measurements on surfaces and bacteria were instantly conducted at room temperature using the sessile drop method with a contact angle meter (Dataphysics OCA 15 Plus, Filderstadt, Germany). Water, formamide, and α-bromonaphthalene (Sigma–Aldrich Co., St. Louis, MO, USA) were used as reference liquids. Three independent assays were performed, with a minimum of five measurements taken for each surface or bacterial substratum. The interfacial free energy (ΔG_{iwi}), apolar (γ_s^{LW}), polar (γ_s^{AB}), Lewis acid (γ_s^+), and Lewis base (γ_s^-) free energy components were calculated based on these measurements.

2.3.4. Raman spectroscopy

Raman spectroscopy was used to study the chemical composition of the bacteria. For this purpose, 10 μL of each bacterial suspension was placed on the top of 1 cm × 1 cm polished silicon wafer coupons (Montco Silicon Technologies Inc., PA, USA) and dried for 1 h at room temperature in a laminar airflow cabinet. Afterward, samples were analysed using a Raman microscope model DXR (Thermo Scientific UK, Ltd., Loughborough, UK) using Omnic software. A 532 nm laser at a power of 1 mW was used with a 50 × objective.

2.4. Biofilm formation assays

Single- and dual-species biofilms of chromosomally tagged *E. coli* and *P. putida* were grown on flat (control), and cauliflower and white cabbage biomimetic wax surfaces using 12-well microtiter plates (CELLSTAR®, Greiner Bio-One, Hillerød, Denmark). First, microtiter plates with double-sided tape adhered to each well, and the downward-facing wax surfaces were UV-sterilized (λ = 253.7 nm) for 1 h in a laminar airflow cabinet. Wax surfaces were then fixed to the wells facing upward and subjected to UV sterilization for 1 h. Subsequently, for single-species biofilms, 3 mL of bacterial suspension prepared in LB, containing ~ 1×10^8 cells mL^{-1} ($OD_{600\ nm} = 0.1$), were added to the microplate wells. For dual-species biofilms, *E. coli* and *P. putida* inocula were added at a 1:1 ratio, resulting in a final cell density of ~ 1×10^8 cells mL^{-1}. Additionally, 3 mL of sterile LB broth medium was added to a well to assess the sterility throughout the assay (negative control). Microplates were then incubated at 25 °C for 24 h under static conditions. Four independent biological assays with two technical replicates each ($n = 8$) were performed.

2.5. Biofilm analysis

As outlined below, single- and dual-species biofilms were analysed by counting the total and culturable cell numbers through flow cytometry and colony-forming unit (CFU) enumeration, respectively. Furthermore, the biofilm architecture and bacterial abundances were studied by confocal laser scanning microscopy (CLSM).

2.5.1. Total cell count

After 24 h of biofilm formation, wax surfaces were carefully removed from the microplate wells, immersed in 4 mL of sterile phosphate-buffered saline, and vortexed for 3 min at maximum speed to obtain biofilm suspensions. The extent of cell removal from the wax surfaces due to vortexing was assessed by SEM (Fig. S1 in Supplementary Material) and was found to be greater than 97%. The numbers of total cells in single- and dual-species biofilms were determined using a FACS Aria IIIu flow cytometer (Becton Dickinson Biosciences, San Jose, CA, USA) equipped with a 488 nm (20 mW) laser connected to a green fluorescence detector (bandpass filter 530/30 nm; used to detect GFP-

expressing *E. coli*) and a 561 nm (50 mW) laser connected to a red fluorescence detector (bandpass filter 610/20 nm; used to detect mCherry-expressing *P. putida*). Bacteria were gated based on their side scatter (SSC) and forward scatter (FSC) signals, and 100,000 events were acquired at a flow rate of 10 μL min^{-1}. Data was analysed using BD FACSDiva software v.6.1.3 (BD Biosciences, San Jose, CA, USA). The results were presented as Log cells per cm^2.

2.5.2. Culturable cell count

To determine the number of culturable cells, biofilm suspensions were serially diluted and spread on LB agar. The plates were incubated overnight at 25 °C for CFU counting. In dual-species biofilms, bacterial strains were discriminated by analysing plates on a blue light transilluminator (DR89X Dark Reader transilluminator, VWR, Søborg, Denmark), which allowed quantification of the number of GFP-expressing *E. coli*. The number of mCherry-expressing *P. putida* was estimated as the difference between the total number of culturable cells and the number of *E. coli* culturable cells. The results were presented as Log CFU per cm^2.

2.5.3. CLSM

The spatial organization and specific bacterial abundances of both single- and dual-species biofilms of *E. coli* and *P. putida* formed on the tested biomimetic surfaces were assessed by CLSM. This analysis was performed using a Zeiss LSM800 microscope (Carl Zeiss Microscopy GmbH, Oberkochen, Germany) equipped with an EC Plan-Neofluar 20 ×/0.50 M27 objective. The *z*-stacks were acquired using Axiocam 503 mono with 488-nm and 561-nm lasers for GFP and mCherry signal detection, respectively. Three stacks (1024 × 1024 pixels, corresponding to 319.45 μm × 319.45 μm) with a *z*-step of 1 μm were recorded for each biofilm sample ($n = 9$). The imaged area per stack was 0.10 mm^2, which corresponded to a total of 0.4% of the coupon area. Three-dimensional (3D) sections of the biofilms were generated using IMARIS 9.3 (Bitplane AG, Zurich, Switzerland). Biofilm parameters, namely biovolume (μm^3 μm^{-2}), thickness (μm), and surface coverage (%) were extracted from CLSM stacks using COMSTAT2. In dual-species biofilms, the relative proportion of each bacterial strain was determined based on the biovolume fractions. The Histo tool provided by the ZEN lite 3.9 software (Carl Zeiss Microscopy GmbH) was also used to trace the intensity values of both fluorescence signals concerning the *z*-position.

2.6. Statistical analysis

Descriptive statistics were used to calculate the mean and standard deviation (SD) for surface roughness, bacterial size, number of biofilm cells, biofilm biovolume, thickness, and surface coverage. Differences in the surface roughness and number of biofilm cells between the flat wax surface (control) and biomimetic wax surfaces were evaluated using the Mann-Whitney test. Quantitative parameters obtained from the CLSM analysis (biofilm biovolume, thickness and surface coverage) were compared using one-way analysis of variance (ANOVA). Statistically significant differences were considered for *p*-values < 0.05. Data was analysed using IBM SPSS Statistics version 29.0 for Microsoft (IBM SPSS, Inc., Chicago, IL, USA).

3. Results and discussion

Several natural surfaces exhibit intrinsic antifouling and antimicrobial properties, essentially due to their topographic features [41]. In this study, biomimetic wax surfaces were produced from two plant leaves, *Brassica oleracea* var. *botrytis* (cauliflower) and *Brassica oleracea capitate* (white cabbage) using a casting technique that has been proven to preserve their main features [28]. The topography and physicochemical properties of the synthesized biomimetic surfaces were characterized and their antibiofilm potential was tested against single- and dual-species biofilms formed by *E. coli* and *P. putida*.

3.1. Topography of biomimetic surfaces

It is known that surface topographic features play a critical role in governing initial bacterial adhesion and biofilm formation [30,41,42]. In this study, scanning electron microscopy was used to visualise the macro topography of the surfaces (Fig. 1). It was demonstrated that the flat surface had some irregular linear features 3 μm–60 μm length and 0.5 μm–1 μm wide (Fig. 1a) that were a result of the moulding process and these features were observed on all the surfaces. Both the CF and WC surfaces clearly demonstrated cellular shaped features, but the CF demonstrated elongated, oval shaped cells with sizes of 40 μm–60 μm length and 15 μm–20 μm wide (Fig. 1b) whilst the WC had much larger cellular shaped features that were almost hexagonal or pentagonal in the shape of 60 μm–150 μm across the diameter of the cell (Fig. 1c).

Optical profilometry was used to examine the topography of the flat (control) and biomimetic wax surfaces, and to quantify their surface roughness using S_a as the measuring parameter (Fig. 2). S_a provides a measure of the average roughness of a surface. The S_a values for both biomimetic surfaces (Fig. 2b and c) were significantly higher than the value of the control wax surface (Fig. 2a, $p < 0.01$). Although there were no statistical differences in the S_a values of the moulded leaf surfaces, the white cabbage surface demonstrated a higher S_a value than the cauliflower surface ($S_{a\ WC} = 4.0 \pm 1.0$ μm versus $S_{a\ CF} = 3.3 \pm 1.0$ μm).

The average size of the maximum peaks and valleys of each surface was also determined (Table S1 in Supplementary Material). As expected, the synthesized biomimetic surfaces possessed larger peak and valley heights than the flat surface (no features). Comparing the two biomimetic surfaces, they presented maximum peaks of similar size ($S_{p\ CF} = 15.0 \pm 4.6$ μm and $S_{p\ WC} = 16.5 \pm 3.3$ μm), although white cabbage had depressions of on average half the size ($S_{v\ CF} = 13.7 \pm 4.4$ μm versus $S_{v\ WC} = 6.7 \pm 2.2$ μm). Regarding the width of the surface profile elements, the average values increased from the flat to cauliflower surface, followed by white cabbage ($R_{sm\ F} = 12.1 \pm 0.7$ μm, $R_{sm\ CF} = 21.1 \pm 2.0$ μm, and $R_{sm\ WC} = 46.4 \pm 2.7$ μm).

Some studies have described a direct association between bacterial binding and increased surface roughness, essentially because rough surfaces have features that may provide favourable sites for colonisation [43,44]. Conversely, other studies have shown that increased surface roughness does not enhance bacterial adhesion [45,46]. Additionally, it has been reported that the association between surface topographic features and bacterial adhesion depends on the size, shape, and density of the microscale features [2,47], and the intrinsic bacterial surface properties [44].

3.2. Physicochemical properties of biomimetic surfaces and bacteria

Bacterial adhesion and biofilm formation on a surface are complex processes influenced by both the type of bacteria and the surface hydrophobicity [25]. The physicochemical parameters of the surfaces and bacteria were determined (Table 1). The interfacial free energy (ΔG_{iwi}) values indicated that the flat wax surface demonstrated hydrophobic properties ($\Delta G_{iwi} = -25.80$ mJ m^{-2}) with lower apolar aspects ($\gamma^{LM} = 33.67$ mJ m^{-2}) and greater polar ($\gamma^{AB} = 12.22$ mJ m^{-2}) and electron Lewis acid and base components ($\gamma^{+} = 3.65$ mJ m^{-2} and $\gamma^{-} = 10.23$ mJ m^{-2}, respectively) than the biomimetic surfaces. The CF surface was the most hydrophobic of the two biomimetic surfaces ($\Delta G_{iwi} = -100.08$ mJ m^{-2}) and although the apolar components of both the biomimetic surfaces were not significantly different ($\gamma^{LM}_{CF} = 38.51$ mJ m^{-2} and $\gamma^{LM}_{WC} = 38.58$ mJ m^{-2}), the CF surface demonstrated less polar, electron Lewis acid and base components (CF = 0.05 mJ m^{-2}, 0.04 mJ m^{-2} and 0.02 mJ m^{-2}; WC = 1.79 mJ m^{-2}, 1.04 mJ m^{-2} and 0.77 mJ m^{-2}, respectively). The hydrophobic behaviour of CF and WC biomimetic wax surfaces was previously demonstrated by Gomes et al. [31]. Plant leaves, including cabbage leaves, are known for their hydrophobic and

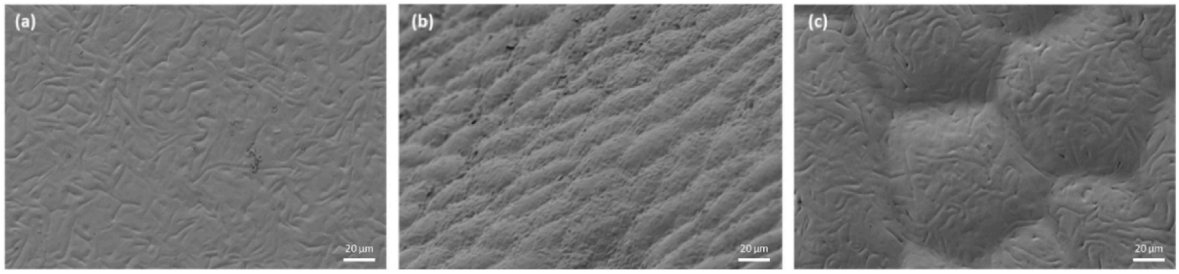

Fig. 1. Scanning electron microscopy images of the surfaces demonstrating differences in the macro topographies of the (**a**) flat, (**b**) cauliflower, and (**c**) white cabbage (magnification of 1000 ×, 20 µm scale bar).

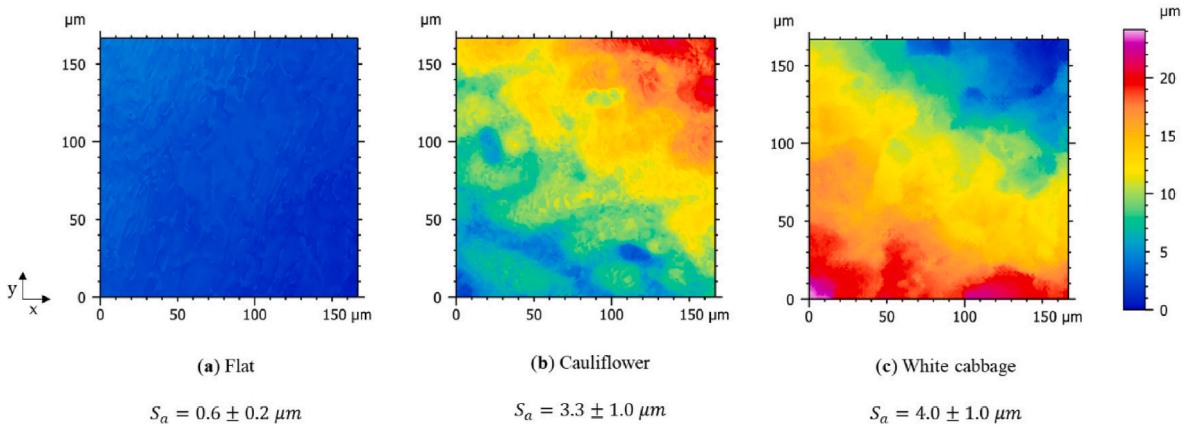

Fig. 2. Two-dimensional (2D) white light profilometry images of (**a**) flat and (**b**, **c**) biomimetic wax surfaces (cauliflower and white cabbage, respectively). The vertical colour bar corresponds to the *z*-range, which represents the surface height range. The average roughness (S_a) values for each surface are presented as the mean ± standard deviation (SD).

Table 1
Physicochemical parameters of the wax surfaces and bacteria.

	ΔG_{iwi} mJ m^{-2}	γ^{LM} mJ m^{-2}	γ^{AB} mJ m^{-2}	γ^{+} mJ m^{-2}	γ^{-} mJ m^{-2}
Surface					
Flat	−25.80	33.67	12.22	3.65	10.23
Cauliflower (CF)	−100.08	38.51	0.05	0.04	0.02
White cabbage (WC)	−71.98	38.58	1.79	1.04	0.77
Bacteria					
E. coli	79.71	25.36	6.74	0.13	86.74
P. putida	39.33	25.71	19.19	1.57	58.69

ΔG_{iwi}, interfacial free energy; γ^{LW}, apolar component; γ^{AB}, polar component; γ^{+}, Lewis acid component; γ^{-}, Lewis base component.

superhydrophobic properties due to the presence of well-ordered micro/nanostructures on their surfaces [25,31,48–50]. Interestingly, our results demonstrated that the most hydrophobic surfaces (WC and CF) had the highest roughness values. This direct association between roughness and hydrophobicity has also been observed in other studies [50,51].

The physicochemical analysis of the bacteria indicated that both strains were hydrophilic, which aligns with the literature [52,53]. *E. coli* was more hydrophilic (ΔG_{iwi} = 79.71 mJ m^{-2}) than *P. putida* (ΔG_{iwi} = 39.33 mJ m^{-2}). *E. coli* was also demonstrated to have lower γ^{AB} and γ^{+} values than *P. putida*.

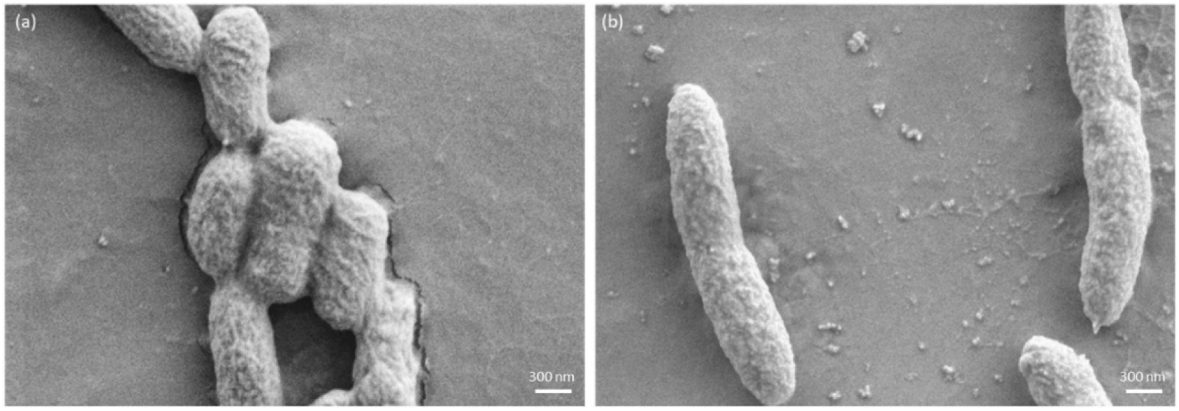

Fig. 3. Scanning electron microscopy of (**a**) *E. coli* and (**b**) *P. putida* cells (magnification of 50,000 ×, 300 nm scale bar).

3.3. Morphology and chemistry of bacterial surfaces

Scanning electron microscopy is a useful tool to determine the size and morphology of the different bacterial species. The bacteria were imaged using SEM to determine their size (Fig. 3). *E. coli* was 2.06 ± 0.36 μm in length by 0.77 ± 0.09 μm width, whilst *P. putida* was 3.78 ± 1.22 μm in length by 0.59 ± 0.04 μm width. The differences in the sizes of the microorganisms are important since their shape has been shown to affect their force of attachment to surfaces [54].

Raman spectroscopy is a method for studying the functional groups and molecules that occur within a microbial cell and provides a wide range of biochemical information of the bacteria in a single spectrum [55]. The analysis of the bacteria demonstrated that different spectral peaks were determined for *E. coli* and *P. putida*. In both bacterial species, spectral peaks were determined at 2722 cm^{-1}, 1580 cm^{-1}, 1349 cm^{-1}, 974 cm^{-1}, 965 cm^{-1}, 946 cm^{-1} and 521 cm^{-1}. In *E. coli*, spectral peaks were found at 451 cm^{-1}, while for *P. putida* they were also identified at 2513 cm^{-1} and 1388 cm^{-1} (Table 2). The cell wall of *E. coli* maintains its rigidity due to murein, which is a complex polymer with roughly equal amounts of polysaccharides (*N*-acetylglucosamine and *N*-acetylmuramic acid), in addition to peptides, L-alanine, D-glutamic acid, L-*meso*-diaminopimelic acid and D-alanine [56]. For *E. coli*, the presence of lipids may correspond to 2722 cm^{-1} and 1349 cm^{-1} and lipopolysaccharides to 965 cm^{-1}, whilst proteins may be potentially assigned at 1580 cm^{-1}, 1349 cm^{-1}, 974 cm^{-1} and 946 cm^{-1}.

P. putida have hydroxylated fatty acids in their composition, and in the outer membrane, they have lipopolysaccharides with hydrocarbon chains, carbohydrates and proteins [56]. For *P. putida*, the presence of lipids may correspond to 977 cm^{-1} and lipopolysaccharides to 962 cm^{-1}, whilst proteins may be potentially assigned at 1388 cm^{-1}, 977 cm^{-1} and 950 cm^{-1}.

The sulphur groups may be due to sulphur-containing amino acids that are found in bacteria, for example, methionine, cysteine, homocysteine, and taurine. In *E. coli* and *P. putida*, spectral peaks that potentially demonstrate sulphur components were identified at 451 cm^{-1} and 521 cm^{-1} for *E. coli* and 2513 cm^{-1} and 521 cm^{-1} for *P. putida*. Methionine is a sulphur-containing amino acid and it is a proteinogenic amino acid and a component of S-adenosyl methionine. The metabolic pathway for its biosynthesis has been extensively characterized in *E. coli* [59]. Cysteine is found in *E. coli* [60] and the sulphur-containing amino acid homocysteine is the last intermediate on the methionine biosynthetic pathway [61]. *P putida* also contains the reverse *trans*-sulphuration pathway, allowing a methionine to cysteine conversion and *P. putida* synthesizes both cysteine and homocysteine [62]. *E. coli* has gene clusters required for the utilization of taurine and alkanesulfonates as sulphur sources [63]. The number of genes involved in sulphur metabolism has been found to be higher in the clinical isolates of *P. putida* than in environmental strains. Hence, the results demonstrated that the molecular species of the two bacteria used in these assays were different, and this is of importance as it influences their surface physicochemistry and may affect the force of binding to surfaces.

Table 2
Raman assignments to *E. coli* and *P. putida* demonstrating the differences in the biochemistry of the bacterial species used in this study.

E. coli (cm^{-1})	*P. putida* (cm^{-1})	Assignment	Ref.
2722		Lipids (CH_2/CH_3)	
	2513	−SH	
1580		Adenine, guanine (ring stretching); –C–O vibration modes—peptidoglycan	[57]
	1388	–COO− symmetric and asymmetric stretching—peptidoglycan	[57]
1349		CH^2 and CH^3—fatty acids and protein deformation; N–H stretching (amide III); C–C stretching—tryptophan; adenine, guanine (ring breathing)	[57]
974	977	C–C stretching protein/=CH lipids	
965	962	C–N stretching (amide lipopolysaccharides)	[58]
946	950	Proteins, phenylalanine, proline	[57]
521	521	S–S stretching	[55]
451		S–S	

3.4. Effect of biomimetic surfaces in single-species biofilms

To evaluate the antibiofilm and antimicrobial potential of the cauliflower and white cabbage biomimetic surfaces, single-species biofilms of *E. coli* and *P. putida* were grown and analysed by quantifying total and culturable cells using flow cytometry analysis and CFU enumeration, respectively, as well as assessing their spatial organization by CLSM. Fig. 4 presents the cell numbers of *E. coli* and *P. putida* single-species biofilms. For *E. coli* biofilms, CF and WC biomimetic surfaces reduced the total cell numbers (live and dead cells) by 50% and 45%, respectively, compared to the control ($p < 0.05$; Fig. 4a), whereas, for *P. putida*, reductions of approximately 60% were obtained for both biomimetic surfaces ($p < 0.05$; Fig. 4c). The results from CFU enumeration (Fig. 4b and d) confirmed the reductions in total cell count, indicating no killing effect. Thus, the tested surfaces act through an antiadhesive mechanism. The changes in the surface roughness and physicochemistry may have affected the number of biofilm cells obtained since these were reduced on the CF and WC species, regardless of the bacterial cell type tested.

The antibiofilm effectiveness of the biomimetic wax surfaces against single-species biofilms was assessed using confocal microscopy. Fig. 5 illustrates representative three-dimensional (3D) structures of single-species *E. coli* and *P. putida* biofilms on flat (control) and cauliflower and white cabbage wax surfaces. *E. coli* (Fig. 5a–c) exhibited a higher biofilm-forming capability, forming denser and thicker biofilms compared to *P. putida* (Fig. 5d–f), as demonstrated by the shadow projections on the right side of the images. Furthermore, 24 h-biofilms of *E. coli* had greater surface coverage than those of *P. putida*, regardless of the tested wax surface. With respect to the effect of surface performance on biofilm formation, both biomimetic surfaces (Fig. 5b–e and c,f) reduced biofilm formation of *E. coli* and *P. putida* compared to the flat surface (Fig. 5a–d).

This qualitative evaluation was confirmed through the biofilm biovolume, thickness, and surface coverage values estimated from confocal image analysis (Fig. 6). The biovolume of *E. coli* biofilms decreased by approximately 40% and 60% on CF and WC surfaces, respectively, compared to the flat surface ($p < 0.001$; Fig. 6a). For *P. putida* biofilms, the CF and WC surfaces had a similar effect on biovolume reduction (approximately 60% decrease; $p < 0.001$). *E. coli* biofilms formed on the biomimetic surfaces also exhibited a decrease in their thickness by 45% compared to those formed on the flat surface ($p < 0.001$; Fig. 6b). Regarding *P. putida* biofilms, only the WC surface significantly reduced the biofilm thickness (30% reduction; $p < 0.05$). Additionally, this biomimetic surface significantly decreased the surface coverage of both *E. coli* and *P. putida* single-species biofilms (approximately 25% and 60% reduction; $p < 0.05$), while the CF surface only reduced *P. putida* biofilm surface coverage (45% reduction; $p < 0.05$; Fig. 6c). Combined, these results corroborate the total cell analysis (Fig. 4) and confirm the potential of biomimetic surfaces, particularly the white cabbage surface, to reduce single-species biofilm formation by *E. coli* and *P. putida*. It may be hypothesised that the distribution of the cells on the surface is a combined effect of the cell properties whereby the smaller, more hydrophilic *E. coli* has resulted in greater biovolume, thickness and surface coverage on the surfaces generally. However, this will be investigated in more detail in future work. The WC demonstrated the lowest biovolume, thickness and surface coverage which may be due to its topography (greatest S_a and largest surface structures), since the chemistry of the surfaces was the same.

Some studies have reported the antifouling effect of biomimetic surfaces against *E. coli*. In a previous study, Gomes et al. [31] revealed

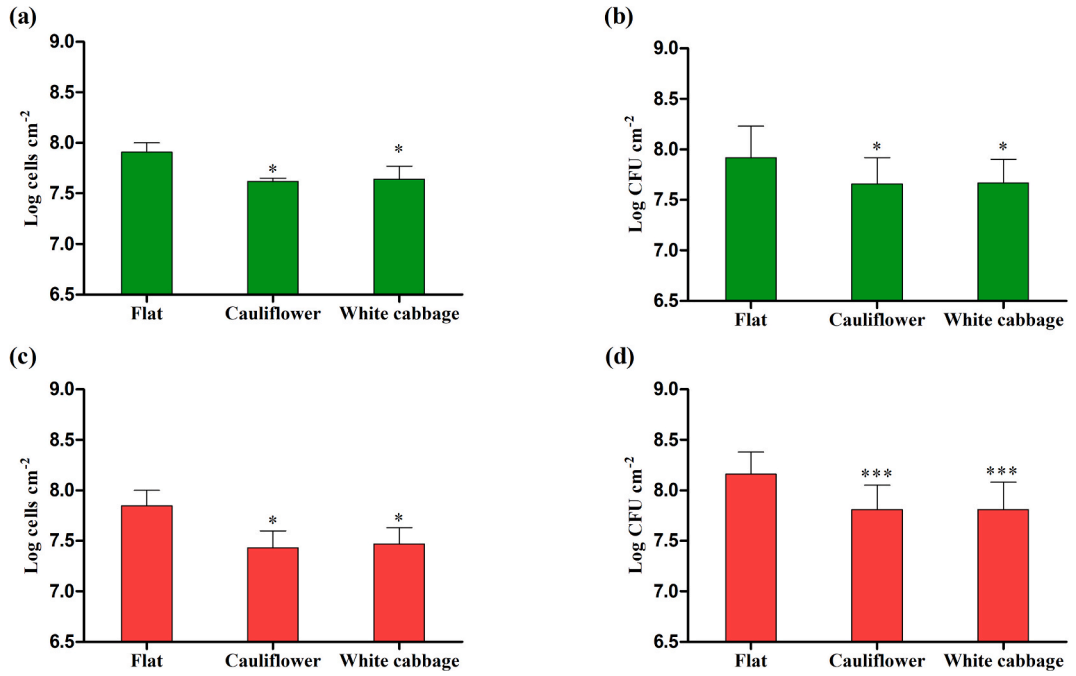

Fig. 4. *E. coli* (green) and *P. putida* (red) (**a** and **c**) total and (**b** and **d**) culturable cells after 24 h of single-species biofilm formation on flat (control), and cauliflower and white cabbage biomimetic surfaces. The number of total cells (both live and dead cells) was quantified by flow cytometry, while the number of culturable cells was determined by CFU enumeration. Results from four independent assays with two technical replicates ($n = 8$) are presented as mean ± SD. Significant differences between the biomimetic surfaces and control were considered for p-values < 0.05 ($^{*}p < 0.05$ and $^{***}p < 0.001$). (For interpretation of the references to colour in this figure legend, the reader is referred to the Web version of this article.)

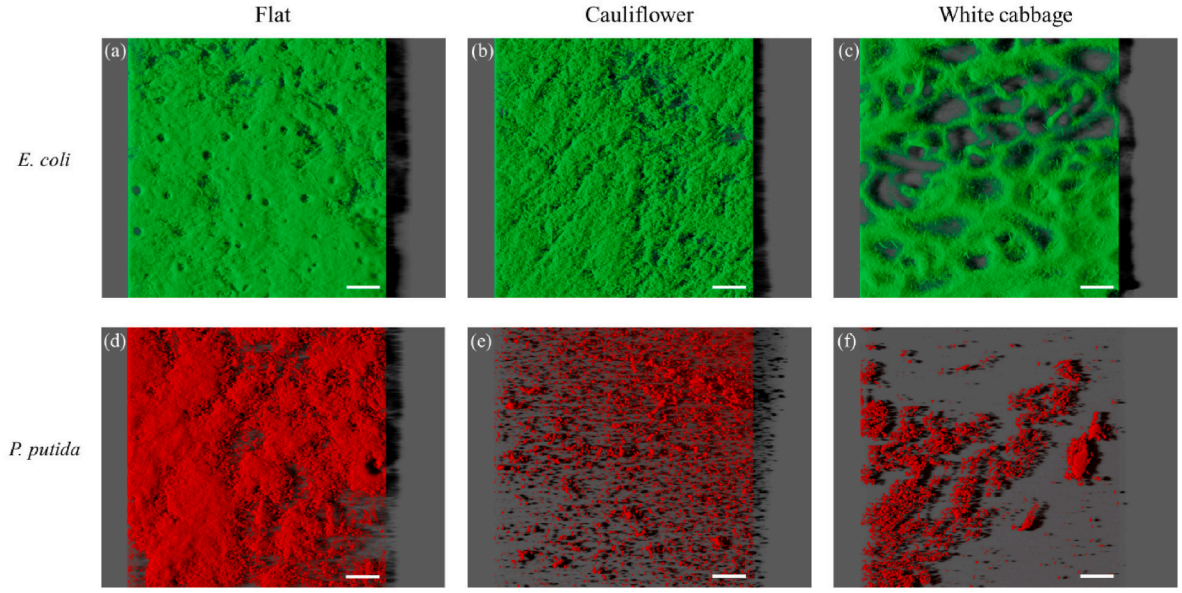

Fig. 5. Single-species biofilms of (**a-c**) *E. coli* (green) and (**d-f**) *P. putida* (red) on flat surface, and cauliflower and white cabbage biomimetic surfaces. These representative images were obtained from confocal *z*-stacks using the IMARIS software and present an aerial, three-dimensional (3D) view of the biofilms. The black shadow on the right represents the vertical projection of biofilm. The white scale bars represent 40 μm.

that the replicated CF and WC wax surfaces reduced the attachment, adhesion, and retention of *E. coli* in comparison to the flat control. The potential of the Gladioli leaf replica surface to repel *E. coli* attachment, adhesion, and retention has also been demonstrated [28]. Gürsoy et al. [51] reported that biomimetic surfaces modified with an antibacterial film and prepared by soft lithography and vapour deposition were able to reduce the *E. coli* culturability by 7-Log in early-stage biofilms. Furthermore, several authors demonstrated the effect of rough shark skin-patterned surfaces in preventing *E. coli* adhesion and biofilm development [46,64]. Likewise, the application of biomimetic surfaces to control biofilm formation by *Pseudomonas* sp. has been reported. Jiang et al. [65] described the antifouling and superhydrophobic behaviour of lotus leaves to repel various bacteria, including *Pseudomonas aeruginosa*. Similarly, the introduction of nanopatterned topographies on hydroxyapatite surfaces resulted in 75% inactivation of *P. aeruginosa* [66].

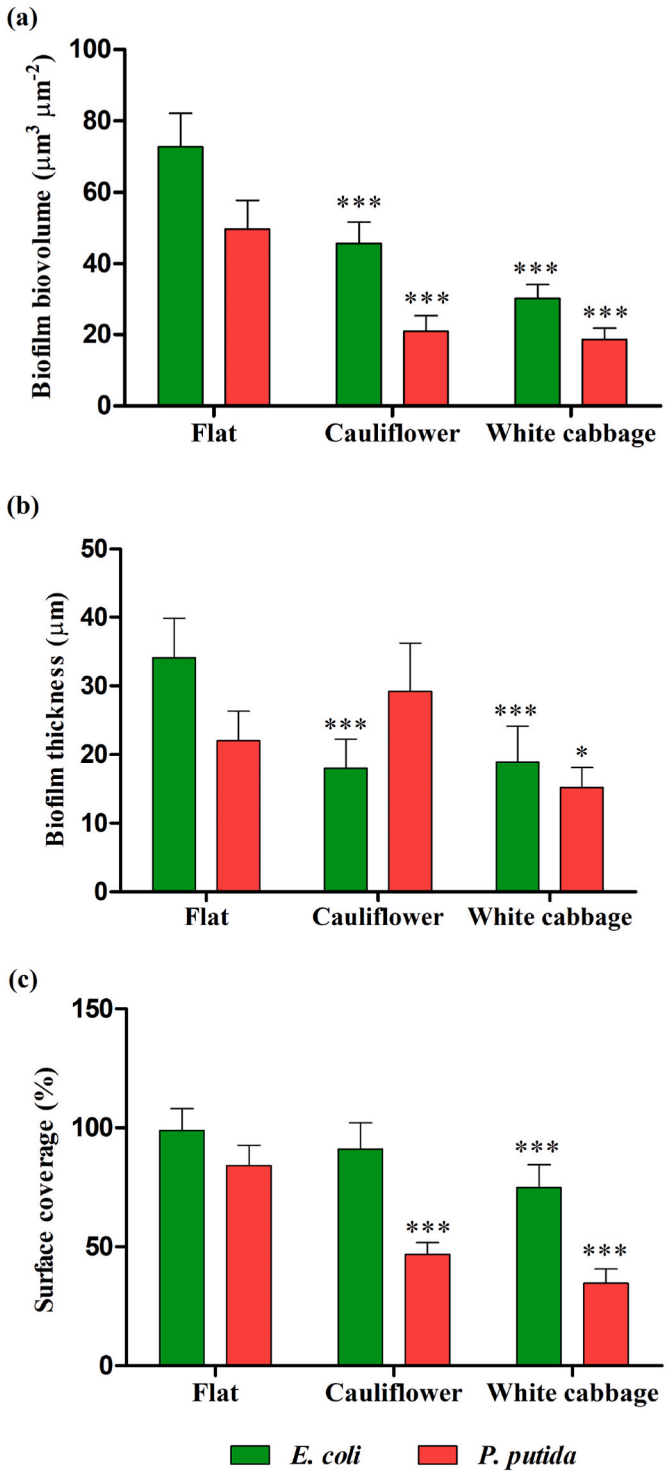

Fig. 6. (**a**) Biovolume, (**b**) thickness, and (**c**) surface coverage of single-species biofilms of *E. coli* (green) and *P. putida* (red) formed on flat surface, and cauliflower and white cabbage biomimetic surfaces for 24 h. The means ± SDs for three independent experiments ($n = 6$) were obtained from confocal image series. Significant differences were considered for $p < 0.05$ (*) and $p < 0.001$ (***).

3.5. Effect of biomimetic surfaces in dual-species biofilms

Biofilms formed on food contact surfaces are composed of numerous microbial species living in proximity, and their interactions may impact biofilm development [2], hence the antibiofilm performance of synthesized biomimetic surfaces was tested against dual-species biofilms formed by *E. coli* and *P. putida*.

Fig. 7 shows the cell composition of dual-species biofilms formed for 24 h on flat, and CF and WC biomimetic surfaces. On average, there was approximately a 40% reduction in the number of total cells in biofilms developed on the WC surface (Fig. 7a). When analysing the composition of mixed biofilms, it was observed that the biomimetic surfaces did not significantly reduce the number of *P. putida* cells. In contrast, the number of *E. coli* cells significantly decreased by approximately 60% on the WC surface compared to the control ($p < 0.05$). Results from CFU enumeration (Fig. 7b) confirmed the reduction in the total *E. coli* cell count observed for the WC surface.

Considering the analysis of the total cell number, biomimetic surfaces exhibited lower antibiofilm efficacy against dual-species biofilms than against single-species biofilms. Therefore, it is important to highlight the performance of the WC surface in reducing *E. coli* cells in dual-species biofilms since, in co-culture, the bacterial species acted differently than when used in single-species biofilms.

To further study the impact of biomimetic surfaces on the biofilm structure and inter-species interactions, dual-species biofilms were evaluated by CLSM. The 3D spatial organization of mixed-species biofilms of *P. putida* and *E. coli* on flat and biomimetic surfaces was determined (Fig. 8). Fig. 8d–i shows the spatial distributions of only *P. putida* and *E. coli* cells, respectively, within the same biofilms. As observed for single-species biofilms (Fig. 5), more biofilm was formed on the control surface compared to the CF and WC biomimetic materials. Moreover, regardless of the tested surface, the bacterial density of dual-species biofilms was lower than that of mono-species biofilms, which was particularly evident for *E. coli* (Fig. 5a–c). From the qualitative confocal microscopy data (Figs. 5 and 8), it was also possible to verify that the biomass of *P. putida* was slightly higher in dual-species biofilms, whereas that of *E. coli* was reduced in the presence of *P. putida* compared to single-species biofilms. The spatial organization of the bacterial strains observed by confocal microscopy revealed similar arrangements in both single- and dual-species biofilms (Figs. 5 and 8). While the flat surface led to the formation of dense and homogeneous biofilms, the biofilms formed on biomimetic surfaces were heterogeneously distributed, with bacteria accumulating more in some areas than in others.

Fig. 9 shows the total (*P. putida* + *E. coli*) and population (*P. putida* or *E. coli)* biovolumes, as well as the average thickness and surface coverage of every dual-species biofilm. The total biovolume ranged from 18 $\mu m^3\ \mu m^{-2}$ (on white cabbage) to 49 $\mu m^3\ \mu m^{-2}$ (on the flat surface) (Fig. 9a), being very similar to that recorded for *P. putida* single-species biofilms and on average 40% lower than the values obtained for *E. coli* single-species biofilms (Fig. 6a). This quantitative result confirmed the antagonistic interaction between *P. putida* and *E. coli*. Furthermore, *P. putida* outgrew *E. coli* in dual-species biofilms, regardless of the surface material (Fig. 9a), which was consistent with the total cell counts (Fig. 7). Approximately 60% of the biovolume of dual-species biofilms corresponded to *P. putida*. Additionally, the proportion of *P. putida*/*E. coli* was similar for the three surfaces tested.

The CF and WC biomimetic surfaces significantly reduced the total biovolume and each of the bacterial populations by approximately 60% compared to the flat surface ($p < 0.001$, Fig. 9a), showing their antibiofilm performance in a more complex setting such as multi-species communities. The same behavior was shown by the surface coverage parameter (Fig. 9c), in which biomimetic surfaces had up to 60% of their area covered, as opposed to the control, which had a surface coverage of 90%. Based on the thickness results (Fig. 9b), the biofilms formed on the CF replicate were approximately half the thickness of those grown on the control surface (17 μm *vs.* 8 μm; $p < 0.001$). In agreement with our work, McClement et al. [28] reported that the ability of the replica Gladioli leaf surface to repel bacteria decreased in co-cultures compared to monocultures of *E. coli* and *L. monocytogenes*. Mixed-species biofilms are generally described as being less susceptible to biofilm control strategies than single-species biofilms [21,22]. Work by others has also shown that

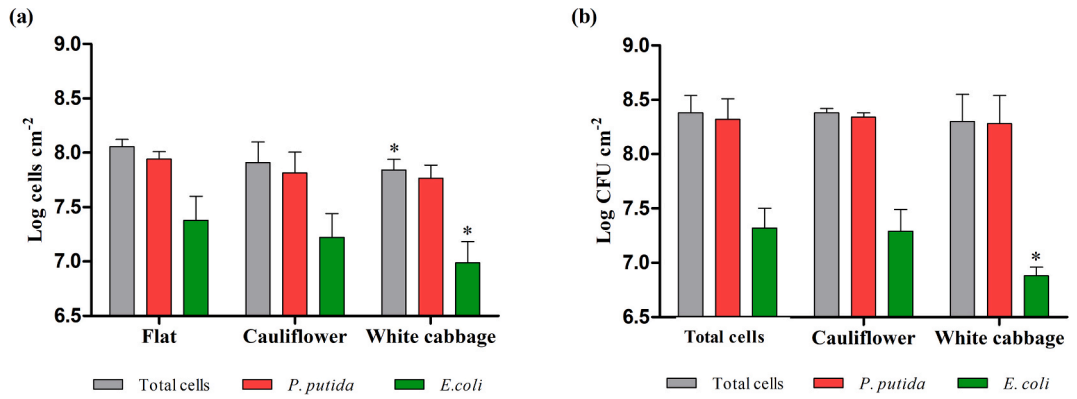

Fig. 7. Cell quantification of 24 h dual-species biofilms formed by *E. coli* (green) and *P. putida* (red) on flat (control), and cauliflower and white cabbage biomimetic surfaces. (**a**) Number of biofilm total and (**b**) culturable cells. Results from four independent assays with two technical replicates ($n = 8$) are presented as mean ± SD. Significant differences between the biomimetic surfaces and control were considered for p-values < 0.05 (*).

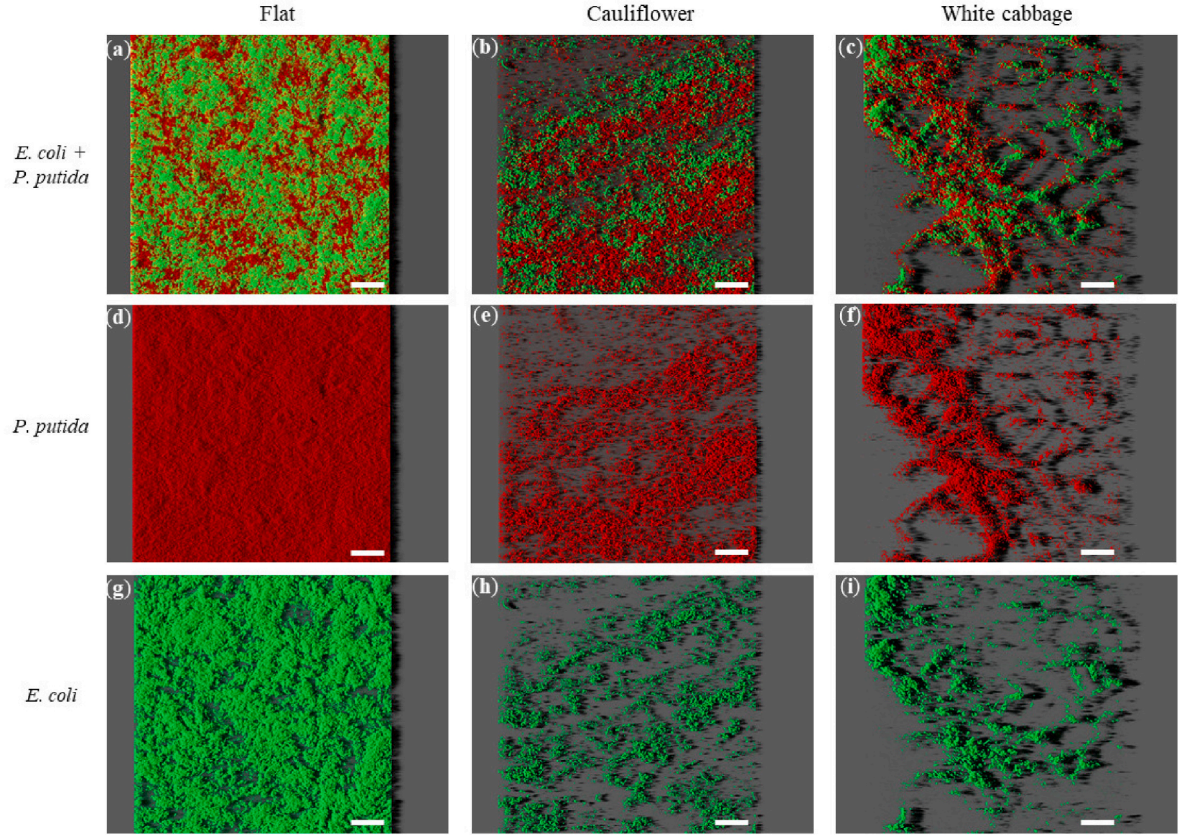

Fig. 8. Dual-species biofilms of *E. coli* and *P. putida* on flat surface, and cauliflower and white cabbage biomimetic surfaces. **(a–c)** presents the combination of red and green filters (*E. coli* + *P. putida*), while **(d–i)** corresponds only to the red (*P. putida*) or green filter (*E. coli*). These representative images were obtained from confocal *z*-stacks using the IMARIS software and present an aerial, three-dimensional (3D) view of the biofilms. The white scale bars represent 40 μm.

bacteria can behave differently when grown in monoculture compared to co-culture [67]. Additionally, results suggest that *E. coli* and *P. putida* strains established a competitive interaction, with *P. putida* having an advantage. Several studies have reported that *Pseudomonas* sp. is dominant in mixed-species biofilms and, generally, hinders the growth of other microorganisms within the consortia [18,21,22,68–70]. Regarding the interaction of *Pseudomonas* spp. and *E. coli*, Cheng et al. [69] demonstrated that *E. coli* growth was negatively affected by the presence of *Pseudomonas* spp. strains in terms of growth fitness and virulence. Additionally, Gomes et al. [70] reported that *Pseudomonas grimontii* inhibited the growth of *E. coli* on food contact surfaces. Cerqueira et al. [71] also reported a dominance of *Pseudomonas* spp. when forming a mixed biofilm with *E. coli*. These authors concluded that the faster growth of *Pseudomonas* strains and eventual production of virulence factors might explain the decrease in *E. coli* biofilm formation. Furthermore, competitive interactions may be antagonistic due to the limitation of nutrient sources and oxygen, and/or by the production of bacteriocins or organic acids that can inhibit the growth of other species [2].

The antagonistic behaviour observed in these multi-species biofilms with *E. coli* has also been observed in previous studies [69,70,72–74] and corroborates the results obtained from biofilm cell analysis. *E. coli*

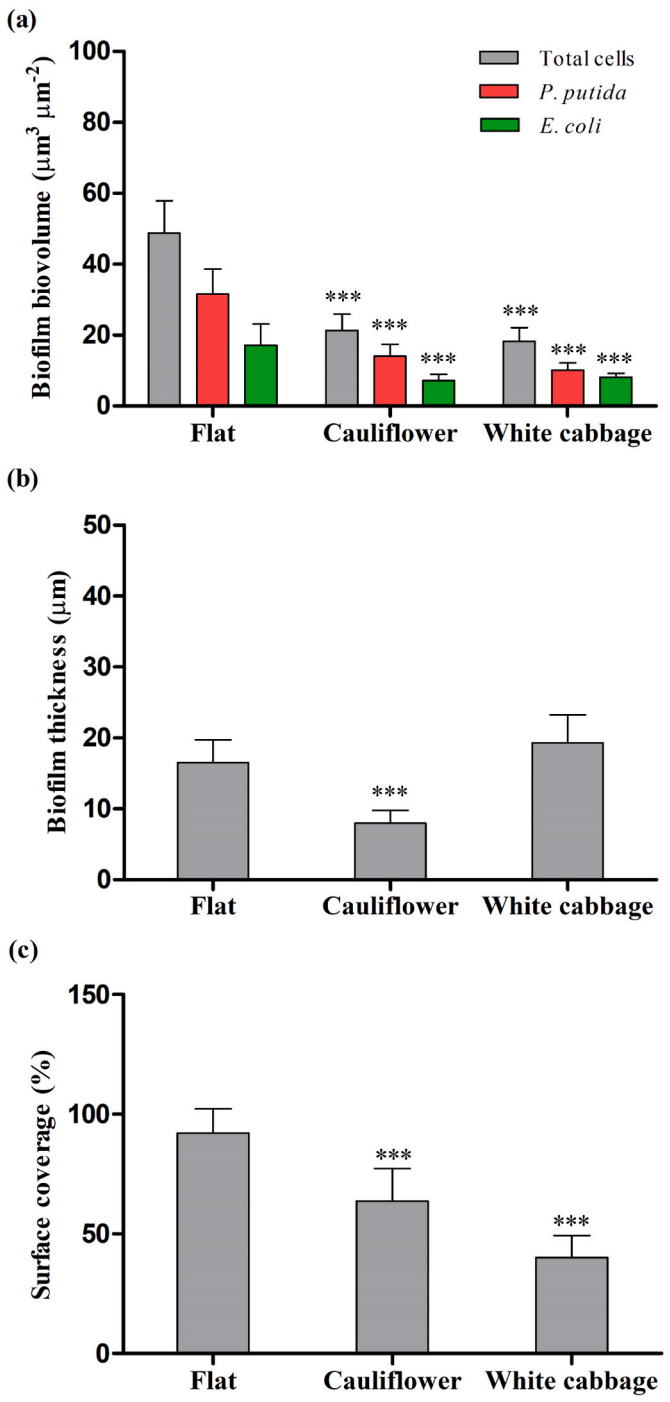

Fig. 9. **(a)** Total and population (*E. coli* or *P. putida*) biovolume, **(b)** thickness, and **(c)** surface coverage of dual-species biofilms on flat surface, and cauliflower and white cabbage biomimetic surfaces. The means ± SDs for three independent experiments ($n = 6$) were obtained from confocal image series. Significant differences were considered for $p < 0.001$ (***).

biofilm formation on solid surfaces was significantly reduced in dual-species cultures with *Staphylococcus epidermidis* [72], *Salmonella* sp. [74], and bacteria isolated from fresh-cut processing facilities such as *Enterobacter cloacae*, *Stenotrophomonas rhizophila*, and *Rhizobium radiobacter* [73].

The vertical spatial organization of the two bacterial strains within the biofilms was determined using CLSM (Fig. 10a). This revealed that *P. putida* and *E. coli* were mostly mixed within the biofilm structures, independent of the materials tested. This was quantitatively validated by the fluorescence profiles along the biofilm (Fig. 10b), in which there was a minor deviation between the two curves. Therefore, in this study, it was found that the competitiveness of *P. putida* against sessile *E. coli* growth was not related to the preferential localization of this bacterium in a specific region of the mixed biofilm, as previously reported by Gomes et al. [70].

Overall, these results suggest that the biomimetic surfaces, especially the replicated WC leaf, exhibited enhanced antiadhesive properties that effectively reduced the amount of single- and dual-species biofilms formed by *E. coli* and *P. putida*. Biomimetic surfaces prevented microbial adhesion, which was reflected in lower surface colonisation (observed by confocal microscopy) and fewer total biofilm cells (assessed by flow cytometry). However, a cell-killing effect was not observed (as demonstrated by viable count number). The mechanism behind the antiadhesive behaviour of these surfaces may be associated with the presence of microscale topographic features that help to reduce the contact area between the cells and the surface and inhibit biofilm formation [25,75]. Additionally, the hydrophobicity of biomimetic materials that have low surface energy can be enhanced by introducing micro/nanostructures on their surfaces. These surfaces typically display the Cassie-Baxter wetting state as a high water contact angle and low contact angle hysteresis enable a droplet to sit on top of the surface features [25,76], reducing the likelihood of bacterial colonisation. Further work is being conducted to gain a deeper understanding of the role of biomimetic surfaces mimicking plant leaves in affecting biofilm formation.

Surface roughness dominated all aspects of the single- and dual-species biofilm formation, whereas surface physicochemistry had the most dominant effect on single-species biofilms. The properties of the cells (e.g., biochemistry and surface hydrophobicity) most affected the biovolume, thickness, and surface coverage of the single- and dual-species biofilms. Although *P. putida* had a competitive effect on *E. coli,* the cells were evenly distributed throughout the biofilm.

The results presented in this study highlight the potential of biomimetic surfaces in reducing biofilm formation by *E. coli* and *P. putida,* which belong to the most prevalent genera found in food processing environments [77]. A 50% reduction in biofilm formation by these bacteria can profoundly impact the operation of a processing unit. A food processing cycle in an industrial unit often starts with a cleaning and disinfection step, which is not aimed at sterilizing the surface as low numbers of bacteria remain [77]. Food processing proceeds until a certain hygienic threshold is reached (risk-based assessment), and then the process stops again for cleaning and disinfection. Cleaning intervals vary within different industries, but values between 4 and 8 h are common in dairies, salad-washing facilities, and meat-processing equipment [78]. Temperatures below 15 °C are also commonly found inside these facilities to curb bacterial growth [79–81]. At these temperatures, doubling times for *E. coli*, *Pseudomonas* sp. and other aerobic bacteria were estimated to be between 4 and 6 h [82–84]. Thus, with a 50% reduction in biofilm formation, the processing time can potentially be extended (in some cases doubled if processing is stopped every 4–6 h) while maintaining the same level of hygiene. The additional processing time enables higher productivity, while the number of daily cleaning cycles could potentially be reduced, resulting in significant economic impacts. This is also extremely important from a sustainable point of view since a reduction in cleaning cycles will result in lower energy, water, and biocide consumption, and a reduction of contaminated effluents in the water system.

The data suggests that the potential of biomimetic surfaces for controlling biofilm formation is promising. However, it is important to comprehensively test their applicability, functionality, and durability before implementation in food processing environments. Furthermore, the dynamics of multi-species biofilm formation were modulated by the bacteria involved in the consortia, emphasizing the importance of conducting multi-species biofilm formation assays when testing antifouling surfaces.

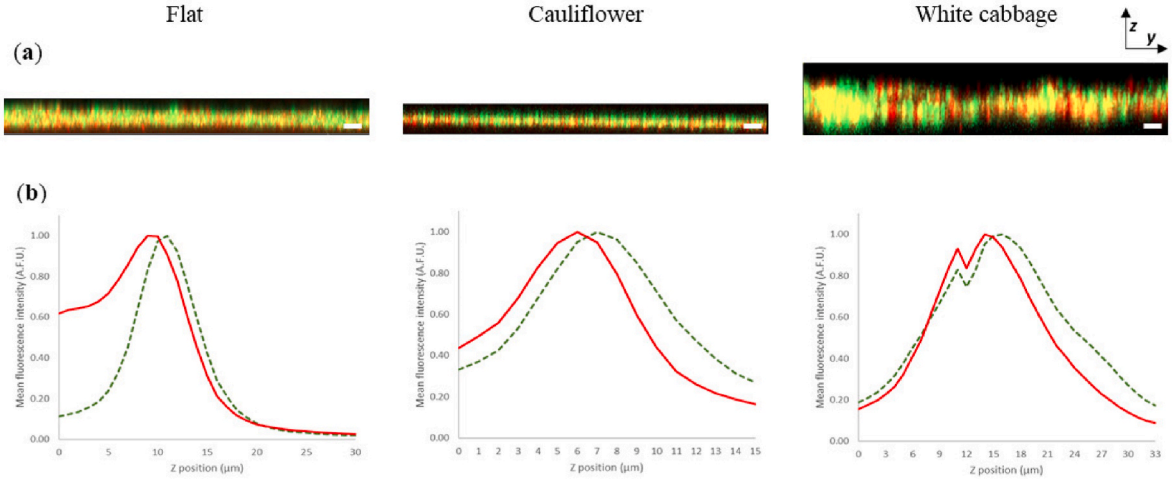

Fig. 10. **(a)** Localization of *P. putida* (in red) and *E. coli* (in green) within dual-species biofilms formed on flat surface, and cauliflower and white cabbage biomimetic surfaces (section views of the CLSM images presented in Fig. 7), and **(b)** distribution of normalized red and green fluorescence intensity values (mean arbitrary fluorescence units (A.F.U.)) along the vertical (*z*) biofilm position (——— - green fluorescence signal, — - red fluorescence signal). The white scale bars represent 40 μm. (For interpretation of the references to colour in this figure legend, the reader is referred to the Web version of this article.)

Funding

This work was supported by national funds through FCT/MCTES (PIDDAC): LEPABE, UIDB/00511/2020 (DOI: 10.54499/UIDB/00511/2020) and UIDP/00511/2020 (DOI: 10.54499/UIDP/00511/2020) and ALiCE, LA/P/0045/2020 (DOI: 10.54499/LA/P/0045/2020); by project SurfSAFE, supported by the European Union's Horizon 2020 Research and Innovation Programme under grant agreement number 952471; and by project 2022.05314.PTDC with DOI 10.54499/2022.05314.PTDC (https://doi.org/10.54499/2022.05314.PTDC), funded by national funds through FCT/MCTES (PIDDAC). Ana Azevedo acknowledges the receipt of a Ph.D. grant from the Portuguese Foundation of Science and Technology (FCT) (2020.07427).

CRediT authorship contribution statement

Rita Teixeira-Santos: Writing – review & editing, Writing – original draft, Formal analysis, Data curation. **Ana Azevedo:** Writing – review & editing, Methodology, Formal analysis, Data curation. **Maria J. Romeu:** Writing – review & editing, Methodology, Formal analysis, Data curation. **Cristina I. Amador:** Writing – review & editing, Validation, Supervision, Methodology, Conceptualization. **Luciana C. Gomes:** Writing – review & editing, Writing – original draft, Project administration, Investigation, Funding acquisition, Formal analysis, Data curation, Conceptualization. **Kathryn A. Whitehead:** Writing – review & editing, Validation, Supervision, Resources, Investigation, Funding acquisition, Conceptualization. **Jelmer Sjollema:** Writing – review & editing, Investigation, Funding acquisition, Conceptualization. **Mette Burmølle:** Writing – review & editing, Supervision, Resources, Investigation, Funding acquisition, Conceptualization. **Filipe J. Mergulhão:** Writing – review & editing, Supervision, Resources, Project administration, Investigation, Funding acquisition, Conceptualization.

Declaration of competing interest

The authors declare the following financial interests/personal relationships which may be considered as potential competing interests:

M.B. is a member of the editorial board for Biofilm. The authors declare that they have no known competing financial interests or personal relationships that could have appeared to influence the work reported in this paper.

Data availability

Data will be made available on request.

Acknowledgments

We would like to acknowledge Anette Løth and Ayoe Lüchau for technical assistance at the University of Copenhagen.

Appendix A. Supplementary data

Supplementary data to this article can be found online at https://doi.org/10.1016/j.bioflm.2024.100185.

References

[1] Srey S, Jahid IK, Ha S-D. Biofilm formation in food industries: a food safety concern. Food Control 2013;31:572–85. https://doi.org/10.1016/j.foodcont.2012.12.001.
[2] Lapointe C, Deschênes L, Ells TC, Bisaillon Y, Savard T. Interactions between spoilage bacteria in tri-species biofilms developed under simulated meat processing conditions. Food Microbiol 2019;82:515–22. https://doi.org/10.1016/j.fm.2019.03.022.
[3] Coughlan LM, Cotter PD, Hill C, Alvarez-Ordóñez A. New weapons to fight old enemies: novel strategies for the (Bio)control of bacterial biofilms in the food industry. Front Microbiol 2016;7. https://doi.org/10.3389/fmicb.2016.01641.
[4] Bouvier L, Cunault C, Faille C, Dallagi H, Wauquier L, Bénézech T. Influence of the design of fresh-cut food washing tanks on the growth kinetics of *Pseudomonas fluorescens* biofilms. iScience 2021;24:102506. https://doi.org/10.1016/j.isci.2021.102506.
[5] Stoodley P, Sauer K, Davies DG, Costerton JW. Biofilms as complex differentiated communities. Annu Rev Microbiol 2002;56:187–209. https://doi.org/10.1146/annurev.micro.56.012302.160705.
[6] O'toole G, Kaplan HB, Kolter R. Biofilm Formation as microbial development. Annu Rev Microbiol 2000;54:49–79. https://doi.org/10.1146/annurev.micro.54.1.49.
[7] Costerton JW, Stewart PS, Greenberg EP. Bacterial biofilms: a common cause of persistent infections. Science 1999;284:1318–22. https://doi.org/10.1126/science.284.5418.1318.
[8] Karygianni L, Ren Z, Koo H, Thurnheer T. Biofilm matrixome: extracellular components in structured microbial communities. Trends Microbiol 2020;28:668–81. https://doi.org/10.1016/j.tim.2020.03.016.
[9] Flemming H-C, Wingender J, Szewzyk U, Steinberg P, Rice SA, Kjelleberg S. Biofilms: an emergent form of bacterial life. Nat Rev Microbiol 2016;14:563–75. https://doi.org/10.1038/nrmicro.2016.94.
[10] Bridier A, Sanchez-Vizuete P, Guilbaud M, Piard JC, Naïtali M, Briandet R. Biofilm-associated persistence of food-borne pathogens. Food Microbiol 2015;45:167–78. https://doi.org/10.1016/j.fm.2014.04.015.
[11] Oliveira GS, Lopes DRG, Andre C, Silva CC, Baglinière F, Vanetti MCD. Multispecies biofilm formation by the contaminating microbiota in raw milk. Biofouling 2019;35:819–31. https://doi.org/10.1080/08927014.2019.1666267.

[12] Li Q, Liu L, Guo A, Zhang X, Liu W, Ruan Y. Formation of multispecies biofilms and their resistance to disinfectants in food processing environments: a review. J Food Protect 2021;84:2071–83. https://doi.org/10.4315/JFP-21-071.

[13] Liu X, Yao H, Zhao X, Ge C. Biofilm Formation and control of foodborne pathogenic bacteria. Molecules 2023;28:2432. https://doi.org/10.3390/molecules28062432.

[14] Carrascosa C, Raheem D, Ramos F, Saraiva A, Raposo A. Microbial biofilms in the food industry-A comprehensive review. Int J Environ Res Publ Health 2021;18. https://doi.org/10.3390/ijerph18042014.

[15] Giaouris E, Heir E, Desvaux M, Hébraud M, Møretrø T, Langsrud S, Doulgeraki A, Nychas GJ, Kačániová M, Czaczyk K, Ölmez H, Simões M. Intra- and inter-species interactions within biofilms of important foodborne bacterial pathogens. Front Microbiol 2015;6:841. https://doi.org/10.3389/fmicb.2015.00841.

[16] Kehe J, Ortiz A, Kulesa A, Gore J, Blainey PC, Friedman J. Positive interactions are common among culturable bacteria. Sci Adv 2021;7:eabi7159. https://doi.org/10.1126/sciadv.abi7159.

[17] Burmølle M, Webb JS, Rao D, Hansen LH, Sørensen SJ, Kjelleberg S. Enhanced biofilm formation and increased resistance to antimicrobial agents and bacterial invasion are caused by synergistic interactions in multispecies biofilms. Appl Environ Microbiol 2006;72:3916–23. https://doi.org/10.1128/aem.03022-05.

[18] Papaioannou E, Giaouris ED, Berillis P, Boziaris IS. Dynamics of biofilm formation by *Listeria monocytogenes* on stainless steel under mono-species and mixed-culture simulated fish processing conditions and chemical disinfection challenges. Int J Food Microbiol 2018;267:9–19. https://doi.org/10.1016/j.ijfoodmicro.2017.12.020.

[19] Elias S, Banin E. Multi-species biofilms: living with friendly neighbors. FEMS Microbiol Rev 2012;36:990–1004. https://doi.org/10.1111/j.1574-6976.2012.00325.x.

[20] Sadiq FA, De Reu K, Steenackers H, Van De Walle A, Burmølle M, Heyndrickx M. Dynamic social interactions and keystone species shape the diversity and stability of mixed-species biofilms - an example from dairy isolates. ISME Commun 2023;3:118. https://doi.org/10.1038/s43705-023-00328-3.

[21] Pang XY, Yang YS, Yuk HG. Biofilm formation and disinfectant resistance of *Salmonella* sp. in mono- and dual-species with *Pseudomonas aeruginosa*. J Appl Microbiol 2017;123:651–60. https://doi.org/10.1111/jam.13521.

[22] Kocot AM, Olszewska MA. Interaction of *Pseudomonas aeruginosa* and *Staphylococcus aureus* with *Listeria innocua* in dual species biofilms and inactivation following disinfectant treatments. LWT 2020;118:108736. https://doi.org/10.1016/j.lwt.2019.108736.

[23] Zhao X, Zhao F, Wang J, Zhong N. Biofilm formation and control strategies of foodborne pathogens: food safety perspectives. RSC Adv 2017;7:36670–83. https://doi.org/10.1039/C7RA02497E.

[24] Hage M, Khelissa S, Akoum H, Chihib NE, Jama C. Cold plasma surface treatments to prevent biofilm formation in food industries and medical sectors. Appl Microbiol Biotechnol 2022;106:81–100. https://doi.org/10.1007/s00253-021-11715-y.

[25] Oopath SV, Baji A, Abtahi M, Luu TQ, Vasilev K, Truong VK. Nature-Inspired biomimetic surfaces for controlling bacterial attachment and biofilm development. Adv Mater Interfac 2023;10:2201425. https://doi.org/10.1002/admi.202201425.

[26] Arango-Santander S. Bioinspired topographic surface modification of biomaterials. Materials 2022;15:2383. https://doi.org/10.3390/ma15072383.

[27] Liu Y, He X, Yuan C, Cao P, Bai X. Antifouling applications and fabrications of biomimetic micro-structured surfaces: a review. J Adv Res 2023. https://doi.org/10.1016/j.jare.2023.08.019.

[28] Mcclements J, Gomes LC, Spall J, Saubade F, Akhidime D, Peeters M, Mergulhão FJ, Whitehead KA. Drawing inspiration from nature to develop anti-fouling coatings: the development of biomimetic polymer surfaces and their effect on bacterial fouling. Pure Appl Chem 2021;93:1097–108. https://doi.org/10.1515/pac-2021-0108.

[29] Yuan Y, Hays MP, Hardwidge PR, Kim J. Surface characteristics influencing bacterial adhesion to polymeric substrates. RSC Adv 2017;7:14254–61. https://doi.org/10.1039/C7RA01571B.

[30] Zheng S, Bawazir M, Dhall A, Kim H-E, He L, Heo J, Hwang G. Implication of surface properties, bacterial motility, and hydrodynamic conditions on bacterial surface sensing and their initial adhesion. Front Bioeng Biotechnol 2021;9. https://doi.org/10.3389/fbioe.2021.643722.

[31] Gomes LC, Saubade F, Amin M, Spall J, Liauw CM, Mergulhão F, et al. A comparison of vegetable leaves and replicated biomimetic surfaces on the binding of *Escherichia coli* and *Listeria monocytogenes*. Food Bioprod Process 2023;137:99–112. https://doi.org/10.1016/j.fbp.2022.11.003.

[32] Saji VS. Wax-based artificial superhydrophobic surfaces and coatings. Colloids Surf, A: Physicochem Eng 2020;602:125132. https://doi.org/10.1016/j.colsurfa.2020.125132.

[33] Moreira JMR, Gomes LC, Whitehead KA, Lynch S, Tetlow LA, Mergulhão FJ. Effect of surface conditioning with cellular extracts on *Escherichia coli* adhesion and initial biofilm formation. Food Bioprocess Technol 2017;104:1–12. https://doi.org/10.1016/j.fbp.2017.03.008.

[34] Meireles A, Fulgêncio R, Machado I, Mergulhão F, Melo L, Simões M. Characterization of the heterotrophic bacteria from a minimally processed vegetables plant. LWT 2017;85:293–300. https://doi.org/10.1016/j.lwt.2017.01.038.

[35] Wang Q, Olesen AK, Maccario L, Madsen JS. An easily modifiable conjugative plasmid for studying horizontal gene transfer. Plasmid 2022;123–124:102649. https://doi.org/10.1016/j.plasmid.2022.102649.

[36] Choi KH, Kumar A, Schweizer HP. A 10-min method for preparation of highly electrocompetent *Pseudomonas aeruginosa* cells: application for DNA fragment transfer between chromosomes and plasmid transformation. J Microbiol Methods 2006;64:391–7. https://doi.org/10.1016/j.mimet.2005.06.001.

[37] Mckenzie GJ, Craig NL. Fast, easy and efficient: site-specific insertion of transgenes into Enterobacterial chromosomes using Tn7 without need for selection of the insertion event. BMC Microbiol 2006;6:39. https://doi.org/10.1186/1471-2180-6-39.

[38] Skovager A, Whitehead K, Wickens D, Verran J, Ingmer H, Arneborg N. A comparative study of fine polished stainless steel, TiN and TiN/Ag surfaces: adhesion and attachment strength of *Listeria monocytogenes* as well as anti-listerial effect. Colloids Surf, B 2013;109:190–6. https://doi.org/10.1016/j.colsurfb.2013.03.044.

[39] Van Oss CJ. Interfacial forces in aqueous media. 2006 [Boca Raton, FL, USA, CRC Press].

[40] Busscher HJ, Weerkamp AH, Mei HCVD, Pelt AWV, Jong HPD, Arends J. Measurement of the surface free energy of bacterial cell surfaces and its relevance for adhesion. Appl Environ Microbiol 1984;48:980–3. https://doi.org/10.1128/aem.48.5.980-983.1984.

[41] Hsieh P-C, Chien H-W. Biomimetic surfaces: insights on the role of surface topography and wetting properties in bacterial attachment and biofilm formation. Colloids Surf, B 2023;228:113389. https://doi.org/10.1016/j.colsurfb.2023.113389.

[42] Francone A, Merino S, Retolaza A, Ramiro J, Alves SA, De Castro JV, Neves NM, Arana A, Marimon JM, Torres CMS, Kehagias N. Impact of surface topography on the bacterial attachment to micro- and nano-patterned polymer films. Surface Interfac 2021;27:101494. https://doi.org/10.1016/j.surfin.2021.101494.

[43] Braem A, Van Mellaert L, Mattheys T, Hofmans D, De Waelheyns E, Geris L, Anné J, Schrooten J, Vleugels J. Staphylococcal biofilm growth on smooth and porous titanium coatings for biomedical applications. J Biomed Mater Res 2014;102:215–24. https://doi.org/10.1002/jbm.a.34688.

[44] Yoda I, Koseki H, Tomita M, Shida T, Horiuchi H, Sakoda H, et al. Effect of surface roughness of biomaterials on *Staphylococcus epidermidis* adhesion. BMC Microbiol 2014;14:234. https://doi.org/10.1186/s12866-014-0234-2.

[45] Moritz J, Abram A, Čekada M, Gabor U, Garvas M, Zdovc I, Dakskobler A, Cotič J, Ivičak-Kocjan K, Kocjan A. Nanoroughening of sandblasted 3Y-TZP surface by alumina coating deposition for improved osseointegration and bacteria reduction. J Eur Ceram Soc 2019;39:4347–57. https://doi.org/10.1016/j.jeurceramsoc.2019.05.051.

[46] Chien H-W, Chen X-Y, Tsai W-P, Lee M. Inhibition of biofilm formation by rough shark skin-patterned surfaces. Colloids Surf, B 2020;186:110738. https://doi.org/10.1016/j.colsurfb.2019.110738.

[47] Wu S, Zhang B, Liu Y, Suo X, Li H. Influence of surface topography on bacterial adhesion: a review. Biointerphases 2018;13:060801. https://doi.org/10.1116/1.5054057.

[48] Muhammad S, Wuyts K, Nuyts G, De Wael K, Samson R. Characterization of epicuticular wax structures on leaves of urban plant species and its association with leaf wettability. Urban For Urban Green 2020;47:126557. https://doi.org/10.1016/j.ufug.2019.126557.

[49] Wang B, Wang J, Yu C, Luo S, Peng J, Li N, Wang T, Jiang L, Dong Z, Wang Y. Sustained agricultural spraying: from leaf wettability to dynamic droplet impact behavior. Glob Chall 2023;7:2300007. https://doi.org/10.1002/gch2.202300007.

[50] Saubade F, Pilkington LI, Liauw CM, Gomes LC, Mcclements J, Peeters M, El Mohtadi M, Mergulhão FJ, Whitehead KA. Principal component analysis to determine the surface properties that influence the self-cleaning action of hydrophobic plant leaves. Langmuir 2021;37:8177–89. https://doi.org/10.1021/acs.langmuir.1c00853.

[51] Gürsoy M, Testici H, Cıtak E, Kaya M, Türk Dağı H, Öztürk B, Karaman M. Biomimetic surfaces prepared by soft lithography and vapour deposition for hydrophobic and antibacterial performance. Mater Technol 2022;37:745–52. https://doi.org/10.1080/10667857.2021.1874760.

[52] Rochex A, Lecouturier D, Pezron I, Lebeault JM. Adhesion of a *Pseudomonas putida* strain isolated from a paper machine to cellulose fibres. Appl Microbiol Biotechnol 2004;65:727–33. https://doi.org/10.1007/s00253-004-1605-7.

[53] Palma-Salgado S, Ku K-M, Dong M, Nguyen TH, Juvik JA, Feng H. Adhesion and removal of *E. coli* K12 as affected by leafy green produce epicuticular wax composition, surface roughness, produce and bacterial surface hydrophobicity, and sanitizers. Int J Food Microbiol 2020;334:108834. https://doi.org/10.1016/j.ijfoodmicro.2020.108834.

[54] Whitehead KA, Rogers D, Colligon J, Wright C, Verran J. Use of the atomic force microscope to determine the effect of substratum surface topography on the ease of bacterial removal. Colloids Surf B Biointerfaces 2006;51:44–53. https://doi.org/10.1016/j.colsurfb.2006.05.003.

[55] Lu X, Al-Qadiri HM, Lin M, Rasco BA. Application of mid-infrared and Raman spectroscopy to the study of bacteria. Food Bioprocess Technol 2011;4:919–35. https://doi.org/10.1007/s11947-011-0516-8.

[56] Brenner DJ, Krieg NR, Staley JT, Garrity GM. Bergey's Manual® of systematic bacteriology. New York, NY: Springer; 2005.

[57] De Siqueira E Oliveira FS, Giana HE, Silveira Jr L. Discrimination of selected species of pathogenic bacteria using near-infrared Raman spectroscopy and principal components analysis. J Biomed Opt 2012;17:107004. https://doi.org/10.1117/1.Jbo.17.10.107004.

[58] De Siqueira E Oliveira FS, Da Silva AM, Pacheco MTT, Giana HE, Silveira L. Biochemical characterization of pathogenic bacterial species using Raman spectroscopy and discrimination model based on selected spectral features. Laser Med Sci 2021;36:289–302. https://doi.org/10.1007/s10103-020-03028-9.

[59] Ferla MP, Patrick WM. Bacterial methionine biosynthesis. Microbiology (Read) 2014;160:1571–84. https://doi.org/10.1099/mic.0.077826-0.

[60] Guédon E, Martin-Verstraete I. Cysteine metabolism and its regulation in bacteria. In: WENDISCH VF, editor. Amino acid biosynthesis - pathways, regulation and metabolic engineering. Berlin, Heidelberg: Springer Berlin Heidelberg; 2007.
[61] Tuite NL, Fraser KR, O'byrne C P. Homocysteine toxicity in *Escherichia coli* is caused by a perturbation of branched-chain amino acid biosynthesis. J Bacteriol 2005;187:4362–71. https://doi.org/10.1128/jb.187.13.4362-4371.2005.
[62] Vermeij P, Kertesz MA. Pathways of assimilative sulfur metabolism in *Pseudomonas putida*. J Bacteriol 1999;181:5833–7. https://doi.org/10.1128/jb.181.18.5833-5837.1999.
[63] Eichhorn E, Van Der Ploeg JR, Leisinger T. Deletion analysis of the *Escherichia coli* taurine and alkanesulfonate transport systems. J Bacteriol 2000;182:2687–95. https://doi.org/10.1128/jb.182.10.2687-2695.2000.
[64] Arisoy FD, Kolewe KW, Homyak B, Kurtz IS, Schiffman JD, Watkins JJ. Bioinspired photocatalytic shark-skin surfaces with antibacterial and antifouling activity via nanoimprint lithography. ACS Appl Mater Interfaces 2018;10:20055–63. https://doi.org/10.1021/acsami.8b05066.
[65] Jiang R, Hao L, Song L, Tian L, Fan Y, Zhao J, Liu C, Ming W, Ren L. Lotus-leaf-inspired hierarchical structured surface with non-fouling and mechanical bactericidal performances. Chem Eng J 2020;398:125609. https://doi.org/10.1016/j.cej.2020.125609.
[66] Iglesias-Fernandez M, Buxadera-Palomero J, Sadowska J-M, Espanol M, Ginebra M-P. Implementation of bactericidal topographies on biomimetic calcium phosphates and the potential effect of its reactivity. Biomater Adv 2022;136:212797. https://doi.org/10.1016/j.bioadv.2022.212797.
[67] Røder HL, Raghupathi PK, Herschend J, Brejnrod A, Knøchel S, Sørensen SJ, Burmølle M. Interspecies interactions result in enhanced biofilm formation by co-cultures of bacteria isolated from a food processing environment. Food Microbiol 2015;51:18–24. https://doi.org/10.1016/j.fm.2015.04.008.
[68] Jahid IK, Mizan MFR, Myoung J, Ha SD. *Aeromonas hydrophila* biofilm, exoprotease, and quorum sensing responses to co-cultivation with diverse foodborne pathogens and food spoilage bacteria on crab surfaces. Biofouling 2018;34:1079–92. https://doi.org/10.1080/08927014.2018.1519069.
[69] Cheng Y, Zhang S, Zhang C, Mi X, Zhang W, Wang L, et al. *Escherichia coli* O157:H7 is challenged by the presence of *Pseudomonas*, but successfully co-existed in dual-species microbial communities. Food Microbiol 2022;106:104034. https://doi.org/10.1016/j.fm.2022.104034.
[70] Gomes LC, Piard JC, Briandet R, Mergulhão FJ. *Pseudomonas grimontii* biofilm protects food contact surfaces from *Escherichia coli* colonization. LWT-Food Sci Technol 2017;85:309–15. https://doi.org/10.1016/j.lwt.2017.03.005.
[71] Cerqueira L, Oliveira JA, Nicolau A, Azevedo NF, Vieira MJ. Biofilm formation with mixed cultures of *Pseudomonas aeruginosa/Escherichia coli* on silicone using artificial urine to mimic urinary catheters. Biofouling 2013;29:829–40. https://doi.org/10.1080/08927014.2013.807913.
[72] Castonguay M-H, Van Der Schaaf S, Koester W, Krooneman J, Van Der Meer W, Harmsen H, et al. Biofilm formation by *Escherichia coli* is stimulated by synergistic interactions and co-adhesion mechanisms with adherence-proficient bacteria. Res Microbiol 2006;157:471–8. https://doi.org/10.1016/j.resmic.2005.10.003.
[73] Liu NT, Nou X, Lefcourt AM, Shelton DR, Lo YM. Dual-species biofilm formation by *Escherichia coli* O157:H7 and environmental bacteria isolated from fresh-cut processing facilities. Int J Food Microbiol 2014;171:15–20. https://doi.org/10.1016/j.ijfoodmicro.2013.11.007.
[74] Chen D, Zhao T, Doyle MP. Single- and mixed-species biofilm formation by *Escherichia coli* O157:H7 and *Salmonella*, and their sensitivity to levulinic acid plus sodium dodecyl sulfate. Food Control 2015;57:48–53. https://doi.org/10.1016/j.foodcont.2015.04.006.
[75] Cheng Y, Feng G, Moraru CI. Micro- and nanotopography sensitive bacterial attachment mechanisms: a review. Front Microbiol 2019;10:191. https://doi.org/10.3389/fmicb.2019.00191.
[76] Cansoy CE, Erbil HY, Akar O, Akin T. Effect of pattern size and geometry on the use of Cassie–Baxter equation for superhydrophobic surfaces. Colloids Surf A Physicochem Eng Asp 2011;386:116–24. https://doi.org/10.1016/j.colsurfa.2011.07.005.
[77] Møretrø T, Langsrud S. Residential bacteria on surfaces in the food industry and their implications for food safety and quality. Compr Rev Food Sci Food Saf 2017;16:1022–41. https://doi.org/10.1111/1541-4337.12283.
[78] Moreira JMR, Fulgêncio R, Alves P, Machado I, Bialuch I, Melo LF, Simões M, Mergulhão FJ. Evaluation of SICAN performance for biofouling mitigation in the food industry. Food Control 2016;62:201–7. https://doi.org/10.1016/j.foodcont.2015.10.023.
[79] Cuggino SG, Posada-Izquierdo G, Bascón Villegas I, Theumer MG, Pérez-Rodríguez F. Effects of chlorine and peroxyacetic acid wash treatments on growth kinetics of *Salmonella* in fresh-cut lettuce. Int Food Res J 2023;167:112451. https://doi.org/10.1016/j.foodres.2022.112451.
[80] Chamberland J, Messier T, Dugat-Bony E, Lessard M-H, Labrie S, Doyen A, Pouliot Y. Influence of feed temperature to biofouling of ultrafiltration membrane during skim milk processing. Int Dairy J 2019;93:99–105. https://doi.org/10.1016/j.idairyj.2019.02.005.
[81] Raab V, Petersen B, Kreyenschmidt J. Temperature monitoring in meat supply chains. Br Food J 2011;113:1267–89. https://doi.org/10.1108/00070701111177683.
[82] Hoel S, Jakobsen AN, Vadstein O. Effects of storage temperature on bacterial growth rates and community structure in fresh retail sushi. J Appl Microbiol 2017;123:698–709. https://doi.org/10.1111/jam.13527.
[83] Lin H, Shavezipur M, Yousef A, Maleky F. Prediction of growth of *Pseudomonas fluorescens* in milk during storage under fluctuating temperature. J Dairy Sci 2016;99:1822–30. https://doi.org/10.3168/jds.2015-10179.
[84] Herendeen SL, Vanbogelen RA, Neidhardt FC. Levels of major proteins of *Escherichia coli* during growth at different temperatures. J Bacteriol 1979;139:185–94. https://doi.org/10.1128/jb.139.1.185-194.1979.